Materials Characterization 95 (2014) 252–258

Contents lists available at ScienceDirect

Materials Characterization

journal homepage: www.elsevier.com/locate/matchar

Characterization of tribo-layer formed during sliding wear of SiC ball against nanocrystalline diamond coatings

Ravikumar Dumpala [a,b], N. Kumar [c], Sunil Kumar Samji [b], S. Dash [c], B. Ramamoorthy [a], M.S. Ramachandra Rao [b,*]

[a] Manufacturing Engineering Section, Department of Mechanical Engineering, Indian Institute of Technology Madras, Chennai 600036, India
[b] Nano Functional Materials Technology Centre, Department of Physics, Indian Institute of Technology Madras, Chennai 600036, India
[c] Indira Gandhi Centre for Atomic Research, Kalpakkam 603102, TN, India

ARTICLE INFO

Article history:
Received 8 March 2014
Received in revised form 21 June 2014
Accepted 28 June 2014
Available online 30 June 2014

Keywords:
Silicon carbide
Nanocrystalline diamond
Tribo-oxidation
Tribo-layer
Characterization

ABSTRACT

Tribo-layer formation and frictional characteristics of the SiC ball were studied with the sliding test against nanocrystalline diamond coating under atmospheric test conditions. Unsteady friction coefficients in the range of 0.04 to 0.1 were observed during the tribo-test. Friction and wear characteristics were found to be influenced by the formation of cohesive tribo-layer (thickness ~ 1.3 μm) in the wear track of nanocrystalline diamond coating. Hardness of the tribo-layer was measured using nanoindentation technique and low hardness of ~1.2 GPa was observed. The presence of silicon and oxygen in the tribo-layer was noticed by the energy dispersive spectroscopy mapping and the chemical states of the silicon were analyzed using X-ray photoelectron spectroscopy. Large amount of oxygen content in the tribo-layer indicated tribo-oxidation wear mechanism.

1. Introduction

Silicon carbide (SiC) is extensively being used as the material for mechanical seals and bearings in hydraulic applications due to its corrosion resistance, wear resistance and thermal stability [1,2]. On the other hand, CVD diamond coatings are emerging as potential materials for such applications because of their unique properties such as chemical inertness, high wear resistance, high thermal conductivity and low friction coefficient [3,4]. Wear and friction properties of these materials are interesting and are the centre of focus due to their potential tribological and mechanical applications [5–7].

Generally, the wear and friction behaviours of the tribo-contact pairs during dry sliding largely depend upon the load, sliding velocity, hardness of the materials and also on the type of interaction, that is, whether it is mechanical or chemical in nature [8]. The contact between two sliding surfaces occurs at asperities and these asperities act as stress concentrators. Purely mechanical wear produces rough contact surfaces and increases the stress concentrations [9]. It is to be noted that the tribo-chemical interactions or tribo-oxidation of the mating parts produce tribo-debris or tribo-layer at the contact interface and decrease stress concentration [9,10]. The tribo-layers of the reaction products are generally softer than the substrate and affect the wear and friction properties, especially under un-lubricated conditions [9,11].

CVD diamond coatings are highly wear resistant and chemically inert while sliding against most of the ceramics and undergo only mechanical wear by means of asperities, fracture and abrasive damage [12]. SiC is considered as one of the non-oxide structural ceramics which is highly resistant against chemical reactions [13]. Even though SiC exhibits excellent chemical inertness in most aggressive environments, it is not the case during tribological interactions. SiC is metastable in the presence of oxygen and understanding the interaction of SiC against CVD diamond during sliding contact is important for exploring the design aspects of effective tribo-systems [14,15]. Instability in the tribochemical wear and tribo-oxidation of SiC under un-lubricated conditions is a well known phenomenon, while sliding against itself or any other hard surfaces [16,17]. Friction and wear behaviour of SiC largely depend upon the nature of the tribo-products formed at the interface, whether tribo-layer or tribo-debris. A stable continuous tribo-layer at the interface acts as a cushion and decreases the contact stress as well as wear due to passive oxidation. Whereas, formation of tribo-debris leads to enhanced wear rates due to active oxidation [18].

In the present study, tribological characteristics of the SiC ball were studied particularly against nanocrystalline diamond (NCD) coatings in mild wear regime using reciprocating tribometer with more emphasis on tribo-layer formation and characterization. Microstructure, thickness, nanohardness and elemental composition of the tribo-layer were studied using different characterization techniques.

* Corresponding author.
E-mail address: msrrao@iitm.ac.in (M.S. Ramachandra Rao).

http://dx.doi.org/10.1016/j.matchar.2014.06.026
1044-5803/

2. Experimental Details

A ball-on-disc type linear reciprocating micro-tribometer (CSM Instruments, Switzerland) was used to study the tribological characteristics of the SiC ball against the flat face of a NCD coated disc under dry test conditions. Pressureless-sintered α-SiC (supplied by CSM Instruments, Switzerland) was selected as the ball (Ø6 mm) material and nanocrystalline diamond (NCD) coated tungsten carbide (WC–Co) flat insert was used as the disc material. Hot filament CVD process was used for the deposition of NCD coating and the details of the NCD growth conditions and experimental setup were discussed elsewhere [19]. The coating thickness was ~3.5 μm and the average grain size was ~60 nm. A normal load of 10 N was used at a sliding speed of 8 cm/s with a stroke length of 3 mm. The friction data was collected at a frequency of 10 Hz. In-situ total penetration depth during the sliding was measured using a linear variable differential transformer (LVDT) sensor coupled to the tribometer.

A confocal Raman microscope (Alpha 300, WITec) was used for the structural characterization of the NCD coating and SiC ball. Spectral data with high resolution of 1 cm^{-1} was obtained using 1800/mm grating at the excitation wavelength of 532 nm. A high resolution scanning electron microscope (Quanta 3D, FEI) was used for the microstructural characterization of the wear track regions. Tribo-layer thickness and the grain size of the NCD coatings were characterized using an atomic force microscope (Dimension EDGE, Bruker). Antimony (n-type) doped silicon tip with nominal radius of curvature ~8 nm was used and AFM scanning was performed in tapping mode. Elemental mapping of the wear track was carried out using an energy dispersive spectroscopy (EDS/Quanta 3D, FEI) technique. Chemical states and composition of the tribo-layer were analyzed by X-ray photoelectron spectroscopy (SPECS FlexMod) coupled with monochromatic Mg Kα radiation at 1253.437 eV. Before the measurements, the XPS instrument was calibrated to the prevailing ISO 15472: 2001 standard [20]. The data are fitted with Lorentzian peaks and background was subtracted using Shirley's method [21].

A triboindenter (TI 950, HYSITRON) instrument loaded with a Berkovich tip of the total included angle of 142.3° and the radius of curvature of 150 nm was used for the hardness measurement. Trapezoidal load cycle was adopted and indentation tests were carried out at 10 mN and 2 mN on the NCD coating and tribo-layer, respectively. Owing to the softness and low thickness of the tribo-layer, low indentation load of 2 mN was chosen for measuring the hardness of the tribo-layer.

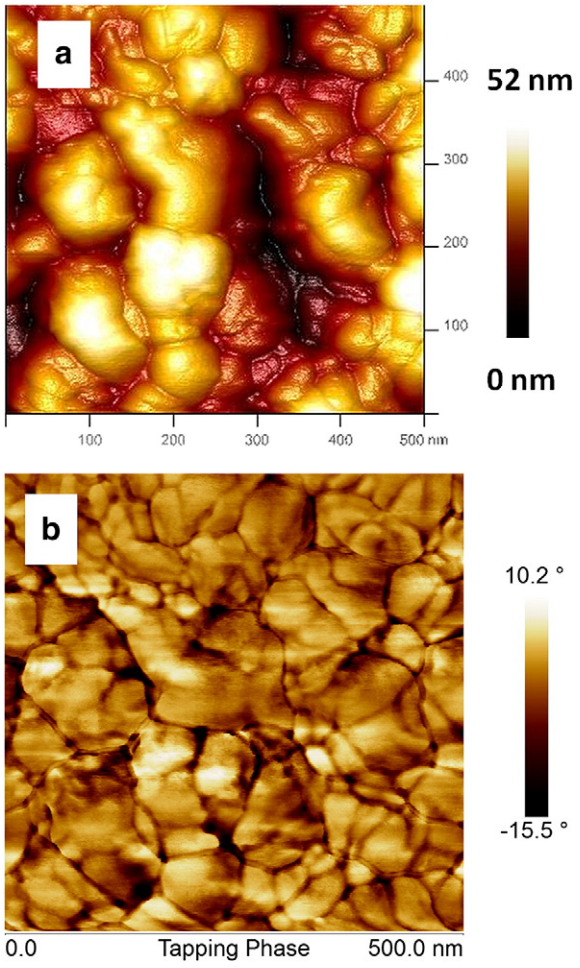

Fig. 1. Surface morphology of the as deposited NCD coating. a) AFM height image, b) AFM phase image. Scan area: 500 × 500 nm.

3. Results and Discussion

3.1. Work Material Characterization

Fig. 1a shows the AFM height image of the as deposited NCD coating, which represents height features of the nanocrystalline diamond grains with ballas type structure. In the tapping mode, the response signal wavelength deviates from the driver signal wavelength, when the probe encounters regions of different compositions. In phase imaging, this phase shift of the response signal (delay in the oscillation) over the driver signal is registered as bright and dark regions, comparable to the way height changes are indicated in the height images. Fig. 1b shows the phase image corresponding to the height image of the as deposited NCD coating. Also in the phase image, the grain boundaries were clearly delineated from the adjacent diamond grains. The average grain size of the NCD coating was ~60 nm, measured from the AFM images.

The Raman spectra of single crystal diamond consists of a Brillouin zone-centre (Γ point) T_{2g} symmetry at 1332 cm^{-1}, however various

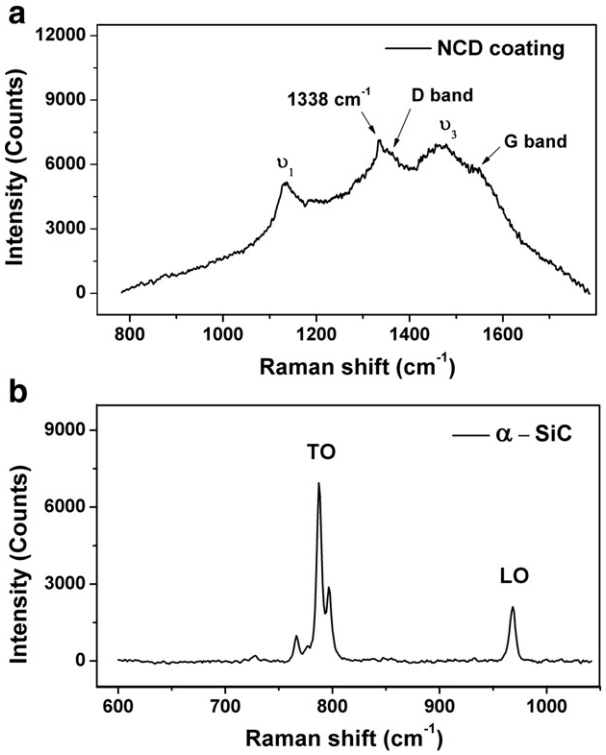

Fig. 2. Raman spectra of a) as deposited NCD coating and b) SiC ball.

other peaks have been observed in the Raman spectra of microcrystalline and nanocrystalline diamond thin films. Raman spectrum of the as deposited NCD film is shown in Fig. 2a. The shift in T_{2g} mode at higher wavenumber (1338 cm^{-1}) signifies compressive stress in the film. Two other peaks were designated as ν_1 and ν_3 which are characteristic of in-plane (C–H) and stretching (C═C) vibrational modes, respectively. The presence of these modes were ascribed to the formation of trans-polyacetylene (TPA) chain present in the grain boundaries and known as characteristic of NCD. The presence of G band signifies E_{2g} symmetry of sp^2C-C bond stretching vibration and D band signifies the breathing mode of A_{1g} symmetry activated by the disorder present in the sp^2C-C bonds originated from the grain boundaries of the NCD coating [22,23].

A typical Raman spectrum of the SiC ball that is shown in Fig. 2b confirms α-SiC phase with hexagonal crystal structure (6-H). Transverse optical (TO, 760 to 800 cm^{-1}) and longitudinal optical (LO, 965 to 975 cm^{-1}) regions were indicated accordingly. Regarding the TO region, α-SiC shows weak Raman peaks at 768 and 796 cm^{-1}, and the strongest at 789 cm^{-1}. Regarding the LO region, α-SiC shows a Raman peak at 967 cm^{-1} [24].

3.2. Friction and Wear Characteristics of the SiC Ball Sliding Against NCD Coating

Fig. 3a and b shows the friction and penetration depth curves of the NCD film sliding against SiC ball and these curves were plotted against

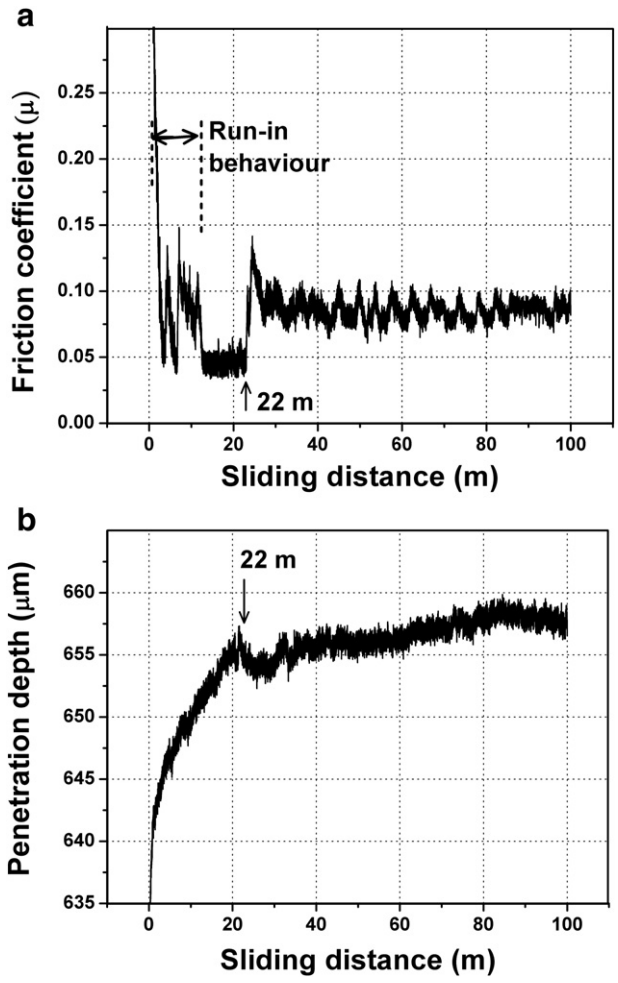

Fig. 3. Tribological characteristics of the SiC ball sliding against NCD coating. Variations of a) friction coefficient and b) penetration depth plotted with respect to the sliding distance.

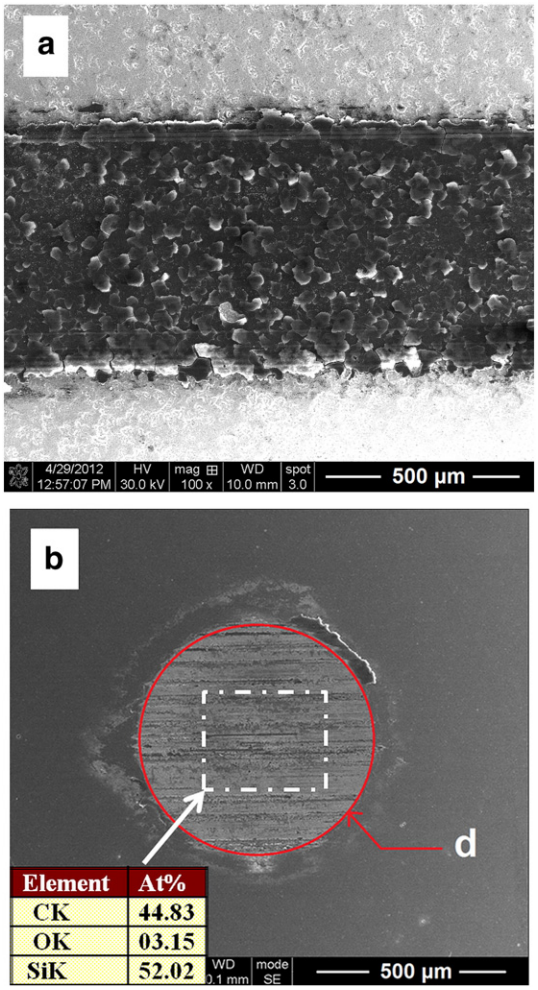

Fig. 4. HRSEM images of the a) wear track on the NCD coating and b) wear scar on the SiC ball recorded after the sliding distance of 100 m. The inset of panel b is the elemental analysis of the marked region obtained using energy dispersive spectroscopy.

the sliding distance of 100 m. Fig. 4a and b shows the HRSEM images of the wear track on the NCD coating and SiC ball wear, respectively after sliding of 100 m. Tribo-layer formation was evident from the HRSEM image of the wear track. Tribo-layer formation was not continuous and it was localized according to the contact asperities and observed as smooth and shiny flakes [25]. High and unstable run-in friction behaviour was observed at the beginning of the test which attributed to the interaction of SiC ball with the sharp asperities of NCD coating. A stable friction coefficient value ~0.04 was observed from the sliding distance starting from 12 m to 22 m. The origin of this low friction coefficient could be due to the direct interaction of SiC ball with the surface of the NCD coating. Because NCD coatings are known for their low friction coefficient, due to the presence of non-diamond graphitic phases (sp^2 hybridized) at the grain boundaries [26].

A sudden jump in the friction co-efficient to 0.1 was observed after a sliding distance of 22 m. This sudden jump in the friction coefficient was attributed to the formation of the stable tribo-layer that was observed in the wear track of the NCD coating (Fig. 4a) [6]. Even though, these tribo-layer products are being generated from the beginning of the tests, a stable tribo-layer was formed only after ~22 m of sliding distance. This stable tribo-layer formation is evident by the dip in the penetration depth exactly after 22 m sliding distance (Fig. 3b). The continuous and rapid wear of the SiC ball was evident from this penetration depth curve. The formation of stable tribo-layer after the sliding distance of 22 m was attributed to the reduced contact pressure due to the increase in

ball wear diameter. The increase in ball wear diameter was evident from the penetration depth curve (Fig. 3b). After the sliding distance of 22 m, the friction co-efficient was observed to fluctuate between 0.07 and 0.1. This periodic instability of the friction coefficient is ascribed to the periodic formation/delamination of the small portions of the tribo-layers. The mechanism of such delaminations after attaining some thickness is governed by the induction of compressive stresses due to multi-cycle sliding. After the sliding distance of 22 m, the tribo-pair could be partially or completely separated by the tribo-layer, which is the main reason for the fluctuating values of friction coefficient. This test has been repeated and the form of the friction curves was found to be similar.

3.3. Wear and Composition Analysis of the NCD Coating and SiC Ball

The average width of the wear track was 720 μm and the SiC ball wear diameter (d) was 694 μm, measured from the respective HRSEM images (Fig. 4a and b). Elemental mapping and analysis of the wear track on the NCD coating covered with tribo-layer were carried out using energy dispersive X-ray spectroscopy (EDS). Fig. 5a shows the secondary electron image of the tribo-layer region. Fig. 5b shows the elemental analysis of that particular region, which shows prominent presence of silicon (Si) and oxygen (O). This indicates the tribo-oxidation of SiC ball, and tribo-products formed during sliding action were transferred to the wear track as tribo-layer due to multi-cycle smearing action [27]. Fig. 5c and d shows the elemental mapping of silicon and oxygen, respectively. The tribo-layer flake features of the secondary electron image (Fig. 5a) match well with the regions of the silicon and oxygen mapping. The uniform presence of the silicon and oxygen suggests that the tribo-layer flakes mainly constitute silicon oxide.

For more accurate analysis, the tribo-layer was characterized by X-ray photoelectron spectroscopy (XPS) to confirm the composition and chemical states [Fig. 6(a)]. In this respect, the XPS spectrum shows two prominent peaks centred at binding energy of 104.6 and 102.4 eV. These peaks correspond to SiO_2 and SiO_x, respectively [28]. The amount of chemical compounds SiO_2 and SiO_x are found to be 75% and 25%, respectively. From this analysis, it is confirmed that the chemical composition of tribo-layer is constituted by silicon oxide. Oxygen peak (O1s) is centred at binding energy of 533.5 eV [Fig. 6b] which determines the formation of silicon oxide as shown in Fig. 6a. The XPS result regarding the presence of oxygen is well corroborated with EDX analysis [Fig. 5b]. The presence of large amount of oxygen appears due to tribochemical reaction.

There is no oxide tribo-layer formation observed on the SiC ball wear scar which was confirmed by the energy dispersive spectroscopy (EDS) analysis details shown in the inset of Fig. 4b. The wear on the SiC ball was mainly due to the second-body abrasion and active tribo-oxidation. During the sliding process, the tribo-products of the SiC ball are transferred to the wear track on the NCD coating. Further, these tribo-products are mechanically smeared and thermally treated during multi-cycle sliding process to form oxide tribo-layer [10]. Wear of the NCD coating was negligible during the sliding test, except the blunting/crushing of sharp asperities/peaks of the NCD coating during the run-in time. Further, the surface of the NCD coating was completely protected by the tribo-layer formed with the aid of oxide tribo-products from the SiC ball. The wear of the SiC ball was mainly due to the tribo-oxidation and the mechanical (abrasive) wear could be happen during

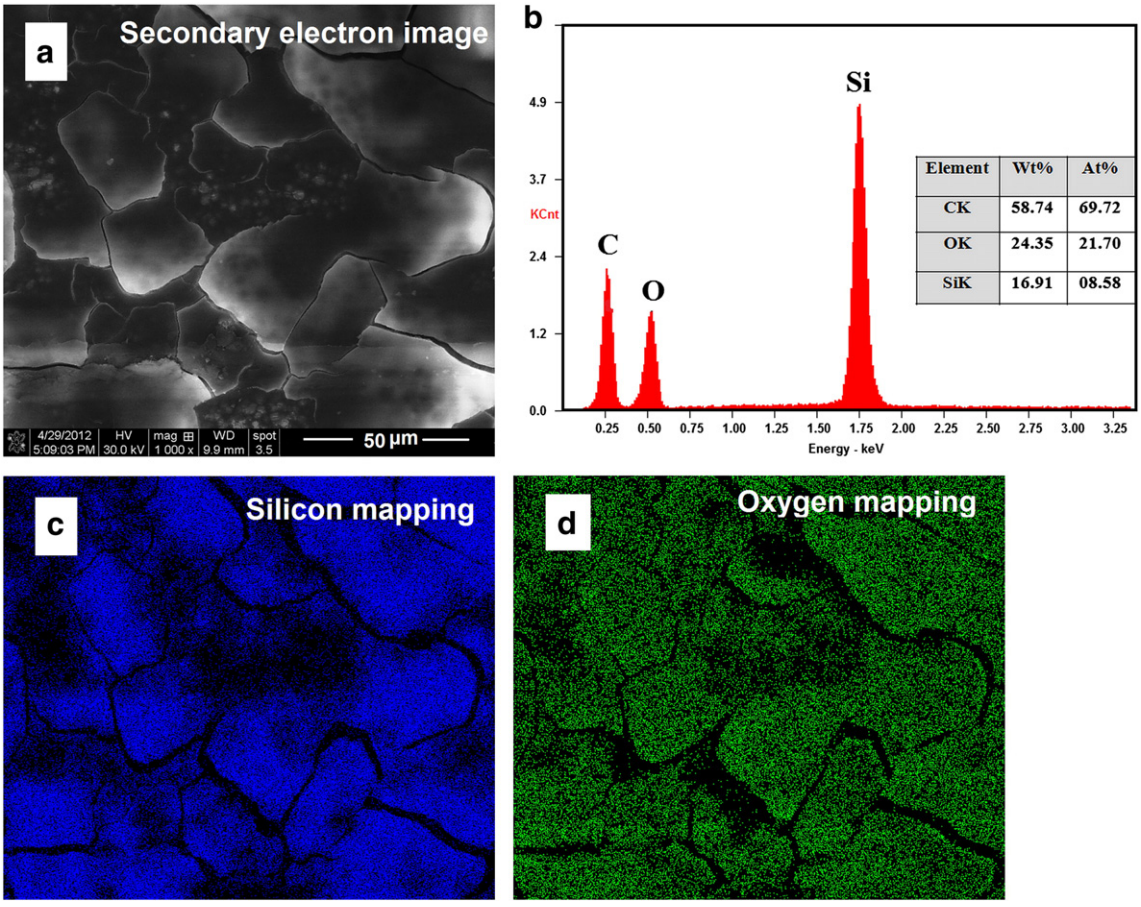

Fig. 5. Elemental analysis and mapping of the tribo-layer formed on the NCD wear track obtained using energy dispersive spectroscopy (EDS). a) Secondary electron image, b) EDS spectrum, c) silicon mapping and d) oxygen mapping.

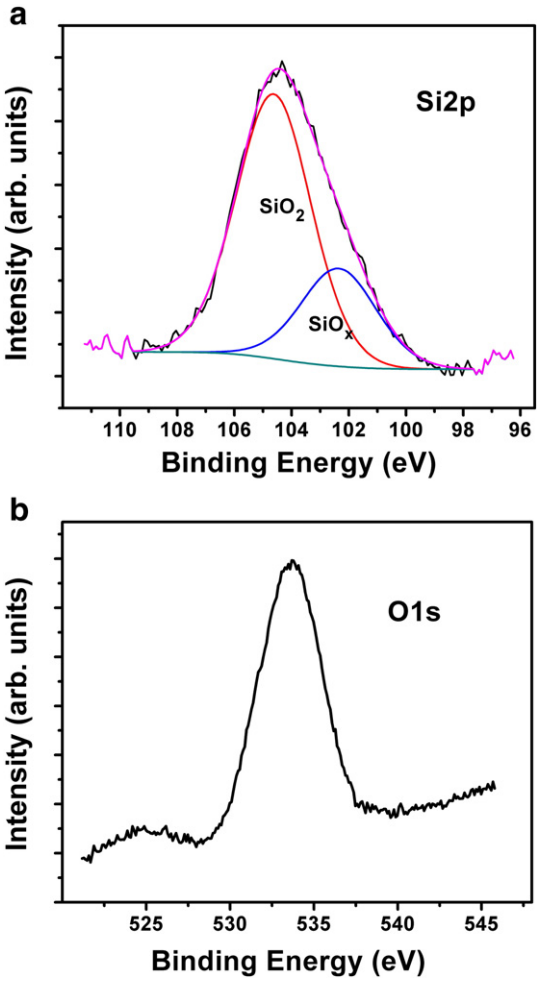

Fig. 6. XPS a) Si2p and b) O1s spectra of silicon oxide tribo-layer.

run-in time due to the interaction with the sharp asperities of the NCD coating. Fig. 3b shows the total wear or penetration depth of the tribo-pair with respect to sliding distance. This penetration depth of approximately 21 μm comprises of both NCD coating and SiC ball wear. Also, SiC ball wear depth (x) of 20.14 μm was measured geometrically from the SiC ball (D = 6 mm) and ball wear diameter (d = 694 μm) as shown in Fig. 7. This result indicates that the total wear depth was mainly contributed by the second-body abrasion and active tribo-oxidation of SiC ball.

SiC ball wear depth calculation (x)

D = Ball diameter, mm

d = Wear diameter, mm

$$y = \sqrt{\left(\frac{D}{2}\right)^2 - \left(\frac{d}{2}\right)^2}$$

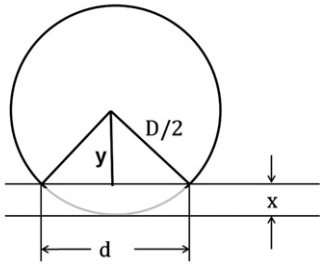

$$\text{Wear depth } (x, \mu m) = \left[\frac{D}{2} - \sqrt{\left(\frac{D}{2}\right)^2 - \left(\frac{d}{2}\right)^2}\right] / 1000$$

Fig. 7. Schematic representation of the SiC ball wear depth calculation.

3.4. Surface Morphology, Thickness and Hardness Details of the Oxide Tribo-Layer

Fig. 8a to c shows the HRSEM images of the wear track regions on the NCD coating at different magnifications, where grey black tribo-layer was evident in the form of flakes. Fig. 8a shows the tribo-layer flakes distributed uniformly and small patches where fresh flakes of tribo-layer were being formed in the delaminated regions. The delaminated regions could be the result of microscopic failure of oxide tribo-layer flakes, due to mechanical and thermal fluctuations caused by continuous compressive smearing action of the SiC ball [10]. Fig. 8b shows the magnified

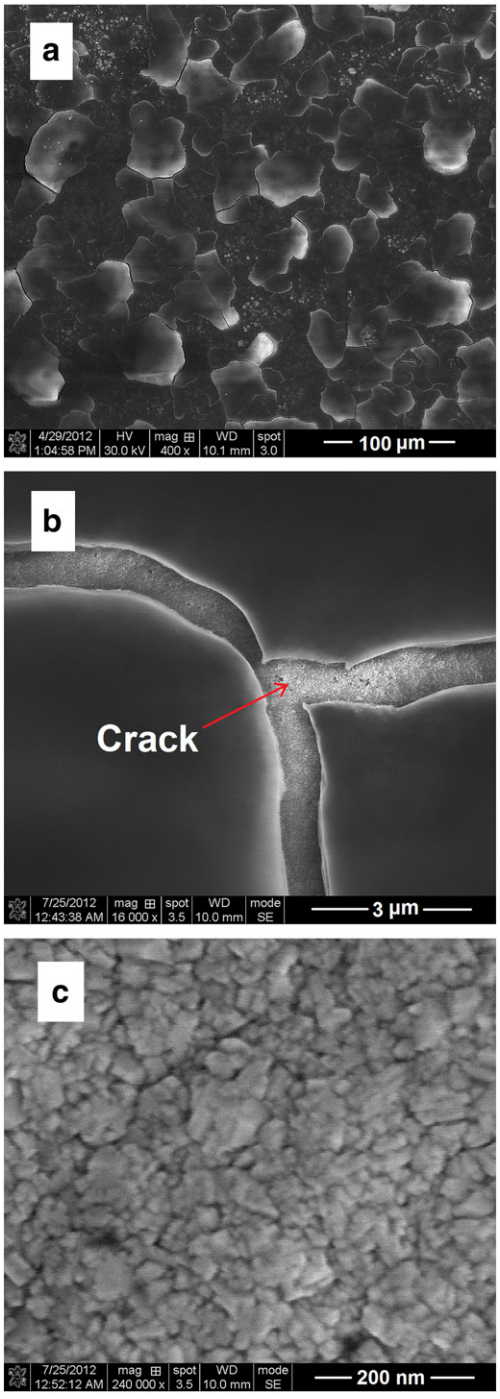

Fig. 8. HRSEM images of the wear track on the NCD coating at different magnifications. a) 400× (tribo-layer flakes), b) 16,000× (cracks in the tribo-layer) and c) 240,000× (exposed NCD coating through the tribo-layer cracks).

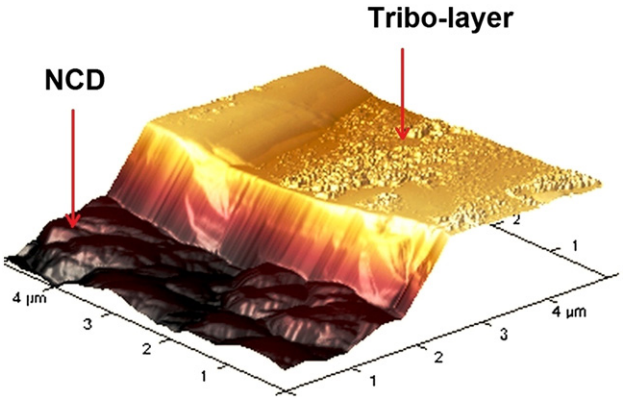

Fig. 9. 3D AFM image of the tribo-layer flake recorded in the wear track of the NCD coating.

regions of the tribo-layer flakes (Fig. 8a) which indicate the smoothness and bring out some microscopic details. Micro-cracks that are observed in the magnified regions of the tribo-layer could be due to thermal quenching and smearing action of the SiC ball. Fig. 8c shows the sub-surface of the tribo-layer seen through the micro-cracks of the flakes, which is the typical morphology of the NCD coating. However, no visible wear signs were observed on the NCD coating, which directly indicates that the NCD coating was being protected by the tribo-layer formation.

Tribo-layer formation starts at the initial contact regions of the tribo-pair and depends upon the rate of oxidation of SiC ball and thereby transferring of tribo-products to NCD coating wear track. The valleys on the NCD coating could have been filled with the oxide tribo-products and smeared during sliding to attain uniformity in the height of wear-track. The thickness of the tribo-layer was not uniform and expected to vary from region to region of the wear track. Fig. 9 shows the 3D AFM image of the delaminated wear track region, which covers both NCD coating and tribo-layer flake. The thickness of the tribo-layer flake at this particular region was measured using sectioning method.

Fig. 10a shows the sectioning of 2D AFM height image to measure the thickness of the tribo-layer at three different positions (A, B and C). Each section of the measurement covers both NCD coating and tribo-layer. Fig. 10b shows the step measurement of A, B, and C sections corresponding to Fig. 10a. The height difference between the NCD coating and tribo-layer surfaces provides the thickness information of the tribo-layer at that particular region. The average thickness of the tribo-layer corresponding to A, B and C sections was ~1.3 μm. Typically, the thickness of the tribo-layer can be up to 3 μm and covers a large portion of the wear track [18].

The average hardness of this silicon oxide tribo-layer was found to be ~1.5 GPa as measured by nanoindentation. This is much less than the NCD coating hardness obtained from the well polished (without formation of oxide layer) NCD surface, which shows a hardness of 40 GPa. Typically, the oxide layer is mild and soft in nature and deforms plastically during indentation [10]. Hence, low indentation load of 2 mN was used for the hardness measurement of oxide tribo-layer. Fig. 11a and b shows the load displacement curves of NCD coating and tribo-layer, respectively. The area under the load displacement curve was large for the tribo-layer (Fig. 11b), which directly indicates the high plasticity of the tribo-layer. Fig. 12 shows the scanning probe image of the Berkovich indents on the silicon oxide tribo-layer obtained during the nanoindentation tests, however no detectable indents were observed on the NCD coating due to high hardness and high elastic modulus.

4. Conclusions

Sliding wear and friction behaviour of SiC ball against flat NCD coated disc were studied under atmospheric test conditions. Unstable friction behaviour was observed throughout the sliding distance and the friction coefficient range from 0.04 to 0.1. HRSEM analysis clearly showed the tribo-layer formation and morphology of the tribo-layer flakes in the wear track of the NCD coating. Elemental mapping of

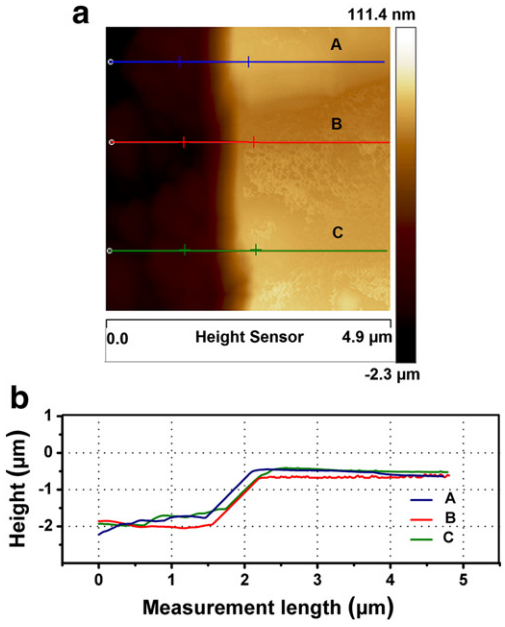

Fig. 10. Tribo-layer thickness measurement. a) Sectioning (A, B and C) of AFM height image and b) sectional step measurement.

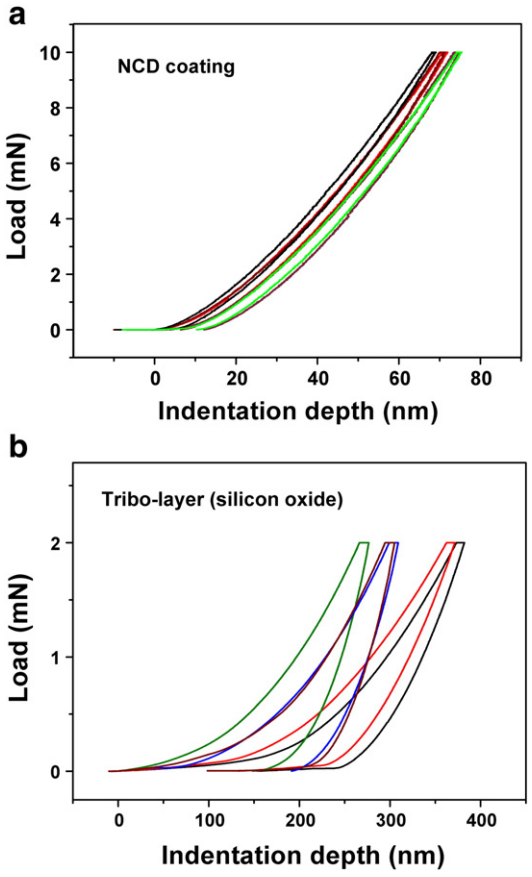

Fig. 11. Load displacement curves obtained during nanoindentation tests on a) NCD coating and b) oxide tribo-layer.

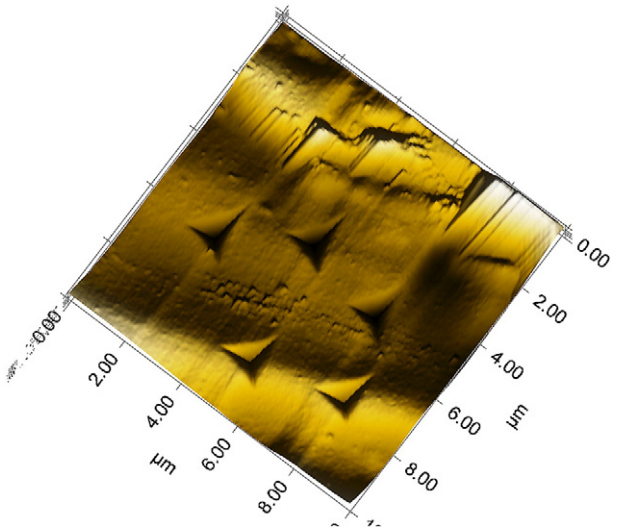

Fig. 12. Scanning probe image of the Berkovich indents obtained during the nanoindentation tests on silicon oxide tribo-layer.

the wear track confirmed the presence of silicon and oxygen in the tribo-layer flakes. The high presence of oxygen was indicative of tribo-oxidation of SiC. X-ray photoelectron spectroscopy study on the tribo-layer confirmed the major presence of silicon dioxide, SiO_2. Thickness of the tribo-layer was 1.3 μm, measured by step method using atomic force microscopy at particular region of the wear track. The tribo-layer was found to be soft as indicated by the low hardness of ~1.5 GPa and the large area under load displacement curve. The formation of this silicon oxide tribo-layer in the wear track is responsible for the unstable friction characteristics of the NCD coating sliding against the SiC ball.

Acknowledgements

MSR would like to thank funding from the Department of Science and Technology (DST), New Delhi that facilitated the creation of Nano Functional Materials Technology Centre (Grant: SR/NM/NAT-02/2005).

References

[1] H. Knoch, M. Fundus, Sintered silicon carbide for slide bearings and seal rings, Seal. Technol. 1995 (1995) 6–14.
[2] X. Wang, K. Kato, K. Adachi, K. Aizawa, Loads carrying capacity map for the surface texture design of SiC thrust bearing sliding in water, Tribol. Int. 36 (2003) 189–197.
[3] M. Amaral, C.S. Abreu, A.J.S. Fernandes, F.J. Oliveira, J.R. Gomes, R.F. Silva, Nanodiamond-based tribosystems, Surf. Coat. Technol. 204 (2010) 1962–1969.
[4] G.A. Jones, D. Arnell, P. Kelly, On the potential of CVD diamond films as mechanical seal face materials, Tribol. Trans. 51 (2008) 33–43.
[5] S. Jahanmir, D.E. Deckman, L.K. Ives, A. Feldman, E. Farabaugh, Tribological characteristics of synthesized diamond films on silicon carbide, Wear 133 (1989) 73–81.
[6] K.H. Zum Gahr, R. Blattner, D.H. Hwang, K. Pöhlmann, Micro- and macro-tribological properties of SiC ceramics in sliding contact, Wear 250 (2001) 299–310.
[7] V. Presser, K.G. Nickel, O. Krummhauer, A. Kailer, A model for wet silicon carbide tribo-corrosion, Wear 267 (2009) 168–176.
[8] V.A. Muratov, T. Luangvaranunt, T.E. Fischer, The tribochemistry of silicon nitride: effects of friction, temperature and sliding velocity, Tribol. Int. 31 (1998) 601–611.
[9] T.E. Fischer, Tribochemistry, Annu. Rev. Mater. Sci. 18 (1988) 303–323.
[10] A. Blomberg, S. Hogmark, J. Lu, An electron microscopy study of worn ceramic surfaces, Tribol. Int. 26 (1993) 369–381.
[11] T.E. Fischer, H. Tomizawa, Interaction of tribochemistry and microfracture in the friction and wear of silicon nitride, Wear 105 (1985) 29–45.
[12] S.J. Bull, Tribology of carbon coatings: DLC, diamond and beyond, Diamond Relat. Mater. 4 (1995) 827–836.
[13] R. Wäsche, D. Klaffke, In situ formation of tribologically effective oxide interfaces in SiC-based ceramics during dry oscillating sliding, Tribol. Lett. 5 (1998) 173–190.
[14] A.V. Sumant, A.R. Krauss, D.M. Gruen, O. Auciello, A. Erdemir, M. Williams, A.F. Artiles, W. Adams, Ultrananocrystalline diamond film as a wear-resistant and protective coating for mechanical seal applications, Tribol. Trans. 48 (2005) 24–31.
[15] P. Hollman, H. Björkman, A. Alahelisten, S. Hogmark, Diamond coatings applied to mechanical face seals, Surf. Coat. Technol. 105 (1998) 169–174.
[16] P. Andersson, A. Blomberg, Instability in the tribochemical wear of silicon carbide in unlubricated sliding contacts, Wear 174 (1994) 1–7.
[17] S. Fan, L. Zhang, L. Cheng, J. Zhang, S. Yang, H. Liu, Wear mechanisms of the C/SiC brake materials, Tribol. Int. 44 (2011) 25–28.
[18] A. Blomberg, M. Olsson, S. Hogmark, Wear mechanisms and tribo mapping of Al_2O_3 and SiC in dry sliding, Wear 171 (1994) 77–89.
[19] R. Dumpala, M. Chandran, N. Kumar, S. Dash, B. Ramamoorthy, M.S.R. Rao, Growth and characterization of integrated nano- and microcrystalline dual layer composite diamond coatings on WC–Co substrates, Int. J. Refract. Met. Hard Mater. 37 (2013) 127–133.
[20] M. Seah, Summary of ISO/TC 201 Standard: VII ISO 15472: 2001 — surface chemical analysis — X-ray photoelectron spectrometers—calibration of energy scales, Surf. Interface Anal. 31 (2001) 721–723.
[21] J. Végh, The Shirley-equivalent electron inelastic scattering cross-section function, Surf. Sci. 563 (2004) 183–190.
[22] A.C. Ferrari, J. Robertson, Origin of the 1150 cm^{-1} Raman mode in nanocrystalline diamond, Phys. Rev. B 63 (2001) 121405.
[23] A.C. Ferrari, Raman spectroscopy of graphene and graphite: disorder, electron–phonon coupling, doping and nonadiabatic effects, Solid State Commun. 143 (2007) 47–57.
[24] H. Okumura, E. Sakuma, J.H. Lee, H. Mukaida, S. Misawa, K. Endo, S. Yoshida, Raman scattering of SiC: application to the identification of heteroepitaxy of SiC polytypes, J. Appl. Phys. 61 (1987) 1134–1136.
[25] K. Holmberg, A. Matthews, H. Ronkainen, Coatings tribology—contact mechanisms and surface design, Tribol. Int. 31 (1998) 107–120.
[26] S.E. Grillo, J.E. Field, The friction of natural and CVD diamond, Wear 254 (2003) 945–949.
[27] C. Zishan, L. Hejun, F. Qiangang, C. Yanhui, W. Shaolong, H. Zibo, Tribological behavior of SiC coating on C/C composites against SiC and WC under unlubricated sliding, Ceram. Int. 39 (2013) 1765–1773.
[28] R. Alfonsetti, L. Lozzi, M. Passacantando, P. Picozzi, S. Santucci, XPS studies on SiO_x thin films, Appl. Surf. Sci. 70–71 (Part 1) (1993) 222–225.